applied sciences

MDPI

Article

Effect of Nitric Acid on the Synthesis and Biological Activity of Silica–Quercetin Hybrid Materials via the Sol-Gel Route

Antonio D'Angelo, Marika Fiorentino, Veronica Viola, Luigi Vertuccio and Michelina Catauro *

Department of Engineering, University of Campania "Luigi Vanvitelli", Via Roma n. 29, 81031 Aversa, Italy; antonio.dangelo@unicampania.it (A.D.); marika.fiorentino@unicampania.it (M.F.); veronica.viola@unicampania.it (V.V.); luigi.vertuccio@unicampania.it (L.V.)
* Correspondence: michelina.catauro@unicampania.it

Abstract: The sol-gel technique stands out as a valuable method for synthesizing biomaterials and encapsulating bioactive molecules, offering potential for controlled drug release and tissue regeneration in biomedical contexts. This study focused on synthesizing silica (Si)-based hybrid biomaterials containing 5% quercetin (Q5) using two different approaches: one involving nitric acid as a catalyst (SiQ5-HNO_3) and the other being acid-free (SiQ5). Structural characterization using Fourier transform infrared (FTIR) and UV-vis spectroscopy revealed oxidation processes compromising the structural integrity of quercetin in both systems. However, it was observed that these oxidation processes led to the formation of oxidized derivatives of quercetin with distinct structures. Additionally, the bioactivity and release kinetics of quercetin from the silica matrices were evaluated, showing that both systems were capable of forming hydroxyapatite, indicating excellent bioactivity. Furthermore, SiQ5 exhibited a higher percentage release of the encapsulated drug at pH 7.4, representing the physiological environment, compared to SiQ5-HNO_3, with a drastic reduction in drug release observed at pH 5.0 (cancer environment). Antibacterial efficacy assessment using the Kirby–Bauer test highlighted the greater antibacterial activity of the SiQ5-HNO_3 system against all tested strains. Overall, this research aims to advance the development of more effective biomaterials for various biomedical applications, particularly in tissue engineering and infection control.

Keywords: sol-gel; silica; quercetin; FTIR; nitric acid; release kinetic; drug delivery; bioactivity; antibacterial study

check for updates

Citation: D'Angelo, A.; Fiorentino, M.; Viola, V.; Vertuccio, L.; Catauro, M. Effect of Nitric Acid on the Synthesis and Biological Activity of Silica–Quercetin Hybrid Materials via the Sol-Gel Route. *Appl. Sci.* **2024**, *14*, 5268. https://doi.org/10.3390/app14125268

Academic Editor: Maria Pia Ferraz

Received: 21 May 2024
Revised: 15 June 2024
Accepted: 17 June 2024
Published: 18 June 2024

Copyright: © 2024 by the authors. Licensee MDPI, Basel, Switzerland. This article is an open access article distributed under the terms and conditions of the Creative Commons Attribution (CC BY) license (https://creativecommons.org/licenses/by/4.0/).

1. Introduction

Bone tissue has the natural ability to self-regenerate after minor traumas or fractures. However, this regenerative capacity is no longer sufficient in the case of large bone defects, often caused by degenerative diseases, severe injuries, or tumors. In such cases, surgical interventions are required to restore the full functionality of the bone [1].

Biomaterials offer innovative solutions for bone and tissue regeneration. These materials, designed to mimic the mechanical and biological properties of tissues, can be implanted in the defect areas to support their growth and regeneration [2].

A wide range of biomaterials are available in the scientific literature, including natural and synthetic polymers, metal oxides, and bioceramics, offering versatile solutions for tissue regeneration [3]. Each biomaterial provides unique characteristics that can be customized to specific tissue engineering needs, paving the way for innovative approaches in regenerative medicine [4].

Indeed, tissue can react to implants with various types of local reactions. The course and effectiveness of implant penetration depend on the structure and shape of the implant. Metal oxides such as titanium alloys have high mechanical strength and do not easily deform or degrade, unlike many of the natural polymers used, which have a short lifespan and are more often used for implants for soft tissue treatment [3]. On the other hand,

metals oxides like titanium are not corrosion-resistant and bond with bone, meaning that the addition of surface coatings is often necessary to increase their bioactivity and corrosion resistance [5].

In this scenario, the choice of bioceramics for treating bone defects provides a good compromise between biocompatibility, biodegradability, strength, osteoconductivity, and osteoinduction. The high hardness and good resistance to abrasion and corrosion in tissue and body fluid environments minimize the wear of ceramic biomaterials after long-term use [6].

Specifically, among these solutions, silica-based bio-glasses can be used for efficient applications in bone tissue engineering as they can enhance revascularization, osteoblast adhesion, enzymatic activity, and the differentiation of mesenchymal stem cells, since they are capable of forming a biologically active hydroxycarbonate apatite layer which is chemically and structurally very similar to the mineral phase of bone and provides an interface that binds to tissues [7].

Silica-based bio-glasses synthesized through the sol-gel method represent a valuable choice for applications in tissue engineering, especially for tissue regeneration post-implantation. The intrinsic ability of the sol-gel method to create porous structures allows for the increased flow of liquids and nutrients through the implanted material, thereby enhancing the adhesion and proliferation of mesenchymal cells. Moreover, the possibility of incorporating bioactive molecules, metabolites, and growth factors into the bio-glass further accelerates the healing process and helps to mitigate the risk of infections and post-implantation inflammation [8–10]. These loaded systems avoid implant rejections through a controlled drug release at the implantation site [11].

Indeed, the sol-gel technique, which concerns a transition from a solution (sol) into a solid matric (gel) through hydrolysis and polycondensation reactions, enables the precise control of the composition and structure of the biomaterials, allowing the development of hybrid bio-glasses with targeted properties [12–14]. This technique, operating at relatively low temperatures, helps to preserve the bioactivity of the incorporated organic molecules, which can further enhance the regenerative process or prevent inflammatory events or bacterial infection [13,15,16]. The sol-gel process is significantly influenced by the presence of acids or bases [12], playing a fundamental role in shaping the characteristics of the resulting gel, impacting various aspects such as reaction speed, gel architecture, and the ultimate properties of the material synthesized. In particular, the acids act as catalysts by accelerating the hydrolysis reaction through electrophilic mechanisms. This acceleration promotes the rapid formation of hydroxyl groups, which are essential for subsequent polymerization reactions [17,18]. In addition, the acid affects the microstructure and properties of the dried and fired gel by favoring linear chain structures [19]. However, the use of acid catalysts, such as nitric acid, can introduce potential drawbacks such as altering the structure and stability of encapsulated bioactive molecules, generating hazardous waste, and posing safety concerns during handling and synthesis [20,21]. Therefore, exploring acid-free synthesis methods is useful for developing safer, more environmentally friendly, and potentially more effective biomaterials.

In this study, silica-based hybrid materials were synthesized by incorporating 5% quercetin (Q5), a flavonol renowned for its anti-inflammatory, antioxidant, and antibacterial properties [22–24]. These properties are mainly due to the presence and placement of the ortho-dihydroxy or catechol group in B-ring, as well as the presence of a 2,3-double bond and a hydroxyl substitution at position 3 and 5 (see structure in Figure 1).

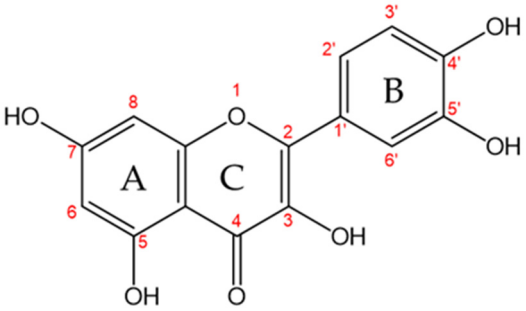

Figure 1. Molecular structure of quercetin.

Two systems were produced by employing two sol-gel-based approaches: one using nitric acid as a catalyst and the other without any acid. This dual approach aimed to investigate the impact of the acidic environment on the structural integrity of quercetin and the overall bioactivity of the hybrid materials.

The rationale behind synthesizing biomaterials with a 5% flavonol content depends on our prior research findings. Through our investigations, we determined that this concentration yielded the most efficient drug release compared to the higher-concentration hybrid materials that we studied. Furthermore, theoretical analyses supported our experimental outcomes, suggesting that at lower drug concentrations, flavonol is well absorbed into the SiO_2 surface with slow mobility. This facilitates the formation of abundant hydrogen bonds between quercetin molecules and the SiO_2 surface, thereby mitigating the formation of agglomerates typically observed at higher concentrations [25,26].

Structural characterization was performed using Fourier transform infrared (FTIR) spectroscopy, while the antibacterial efficacy was assessed through the Kirby–Bauer antibacterial sensitivity test. Additionally, the bioactivity and release kinetics of quercetin from the silica matrices were studied to evaluate their potential as drug delivery systems. Similar studies have demonstrated the effectiveness of the sol-gel technique for drug delivery, such as the encapsulation of antibiotics in silica matrices to control infection, the release of anti-inflammatory drugs for sustained therapeutic effects, and the incorporation of anticancer agents to target tumor cells [27–29]. The findings from this research could contribute to the development of more effective biomaterials for biomedical applications, particularly in tissue engineering and infection control.

2. Materials and Methods

2.1. Synthesis via the Sol-Gel Route

The sol-gel method was used to synthesize a silica structure loaded with 5% quercetin (Q) using two different approaches. Tetraethyl orthosilicate (TEOS), from Sigma-Aldrich in Darmstadt, Germany, served as the silicate precursor. The TEOS was dissolved in a solution of ethanol (99.8%, Sigma-Aldrich) and distilled water under continuous magnetic stirring to ensure homogeneity. In one approach, a solution of quercetin (Q) from Sigma-Aldrich, solubilized in ethanol, was added to the silicate solution. Nitric acid was then introduced to speed up reactions [17,18], resulting in a hybrid system called SiQ5-HNO_3. Ratios used for the synthesis are all reported in [30] and were as follows: TEOS/EtOH/H_2O/HNO_3/Q = 1:6:4:0.6:0.034. In the other approach, the synthesis was carried out without acid, leading to another hybrid system designated as SiQ5 (following the same molecular ratio). After successful gelation, the samples were dried at 50 °C for 24 h, forming a glass material. As a comparison, SiO_2 samples without encapsulated quercetin were also synthesized both in the presence (labelled as Si-HNO_3) and absence (labelled as Si) of nitric acid, following both the same molar ratios and synthesis protocol. The synthesis process and images of the gels and resulting SiQ5 and SiQ5 HNO_3 glasses are illustrated in Figure 2.

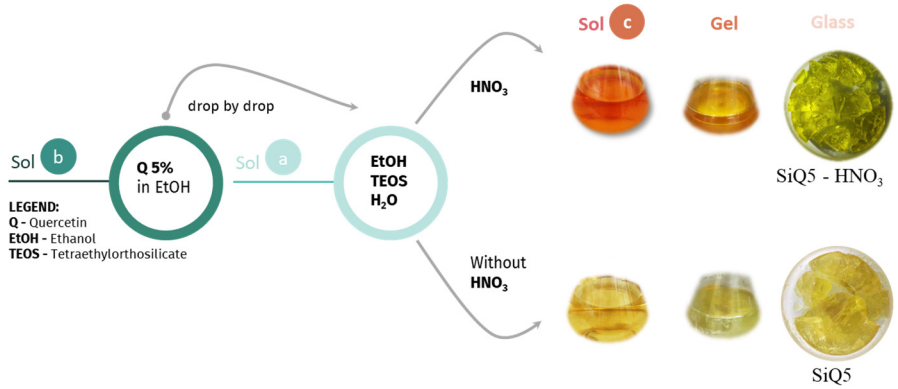

Figure 2. Flowchart depicting the synthesis of SiQ5 with and without HNO_3.

2.2. Characterization of Hybrid Materials

2.2.1. FTIR Characterization

FTIR analysis was performed using the Prestige21 Shimadzu system (Shimadzu Italia S.R.L., Milan, Italy), equipped with a DTGS KBr detector (Shimadzu Italia S.R.L., Milan, Italy), with a resolution of 2 cm^{-1} (60 scans), within the range of 400–4000 cm^{-1}. KBr disks (2 mg sample and 198 mg KBr) were utilized in the analysis procedure. The obtained FTIR spectra were processed using IRsolution (v.160, Shimadzu, Milan, Italy) and Origin 8 (v.2022b, OriginLab Corporation, Northampton, MA, USA) software. The spectra of the inorganic silicate structure and quercetin in the presence and absence of HNO_3 were used as comparisons for the hybrid systems.

2.2.2. Bioactivity Study of Silica/Quercetin System

The in vitro bioactivity study was conducted following the methodology proposed by Kokubo et al. [31]. Discs weighing 250 mg each of every sample were prepared and immersed in simulated body fluid (SBF) for 7, 14, and 21 days. SBF mimics the inorganic ion composition of human plasma and was prepared by dissolving NaCl, $NaHCO_3$, KCl, $MgCl_2 \cdot 6H_2O$, $CaCl_2$, Na_2HPO_4, and Na_2SO_4 (purchased from Sigma-Aldrich) in ultrapure water. The solution was buffered to pH 7.40 using 4-(2-hydroxyethyl)piperazine-1-ethanesulfonic acid hemisodium salt (HEPES, Sigma-Aldrich) and NaOH. Disk samples and SBF were contained in polystyrene bottles placed in a static water bath set at 37.0 ± 0.5 °C. A powder-to-solution ratio of 250 mg/50 mL was maintained. To prevent the depletion of ionic species in the SBF and counteract the nucleation of biominerals on the samples, the solution was refreshed every 2 days. Following an exposure period of up to 21 days, the samples were withdrawn from the SBF, rinsed gently with distilled water, and subsequently dried in a desiccator. The evaluation of hydroxyapatite was performed by using FTIR analysis (following the procedure of the previous paragraph). Moreover, microstructural information of samples after 21 days of soaking in SBF was acquired through scanning electron microscopy (SEM, Quanta 200, FEI, Eindhoven, The Netherlands) and energy dispersive X-ray spectroscopy (EDS) analysis.

2.2.3. Encapsulation Efficiency and Drug Release Study

The encapsulation efficiency loading of Si-Q5 and SiQ5-HNO_3 was evaluated by calculating the mass ratio of the total amount of encapsulated drug to the initial drug amount added to Si and Si-HNO_3 matrices. To calculate the total amount of the encapsulated drug, 5 and 10 mg of SiQ5 and SiQ5-HNO_3, respectively, were mixed with 5 mL of ethanol and underwent ultrasound-accelerated maceration for 30 min using an ultrasound bath Elmasonic S 15 H (Elma Schmidbauer GmbH, Singen, Germany) and centrifuged for 10 min at 3000× *g* [32]. The supernatants were analyzed using a T65 UV-visible Spectrophotometer PG instruments (Leicestershire, UK) at 253 nm for SiQ5 and 299 nm for SiQ5-HNO_3. A cali-

bration curve was built for quercetin extracted using SiQ5 and SiQ5-HNO_3 from 5.0 mg/mL to 35 mg/mL. The encapsulation efficiency (EE%) was calculated using the formula:

$$\mathbf{EE}(\%) = \frac{\mathbf{Wt}}{\mathbf{Wi}} \times 100$$

where Wt is the total mass of the incorporated quercetin and Wi is the total quercetin mass added initially during the sol-gel synthesis [33].

Successively, kinetic measurements of quercetin drug release from SiQ5 and SiQ5-HNO_3 were carried out in SBF at pH 7.4 and 5.0 at 37 °C using a T65 UV-Visible Spectrophotometer with a wavelength range of 190–1100 nm and an 8-cell motorized cell changer, purchased from PG instruments, Leicestershire (UK). The release kinetics were studied in simulated body fluid (SBF) at pH 7.4 to mimic the physiological conditions of a healthy cellular environment, and at pH 5.0 to simulate the conditions found in tumor cells [34]. For the SiQ5 system synthesized without a catalyst, a calibration curve of standard quercetin was constructed based on its λ max at 253 nm at pH 7.4 and 5.0, yielding an R^2 value of 0.9975 and 0.9995, respectively. For the silica system synthesized in the presence of nitric acid, previous studies demonstrated that quercetin undergoes oxidation during the encapsulation process, and its oxidized form was utilized to monitor the release in the presence of acid. A calibration curve of oxidized quercetin was established by measuring the absorbance of a standard concentration of oxidated quercetin prepared in SBF at pH 7.4 and 5.0 and correlating the solution concentrations with absorbance at a wavelength of 299.0 nm, resulting in an R^2 value of 0.9978 and 0.9994, respectively (Figure 3). The concentration range covered was from 5.0 mg/L to 35.0 mg/L. For the release test, 15 mg of both SiQ5 and SiQ5-HNO_3 were solubilized in 25 mL of SBF solution at pH = 7.4 and pH 5.0 alternately while being continuously stirred and then centrifuged. The supernatant was collected for quantification via UV-Vis. The percentage quercetin release was calculated with respect to the incorporated amount of drug determined by EE for the SiQ5 and SiQ5-HNO_3. The absorbance of quercetin was measured in accordance with each calibration curve in triplicate at time intervals of 0, 0.5, 1, 2, 3, 4, 5, 6, 7, 8, and 24 h, and the outcomes were extrapolated using the calibration curve.

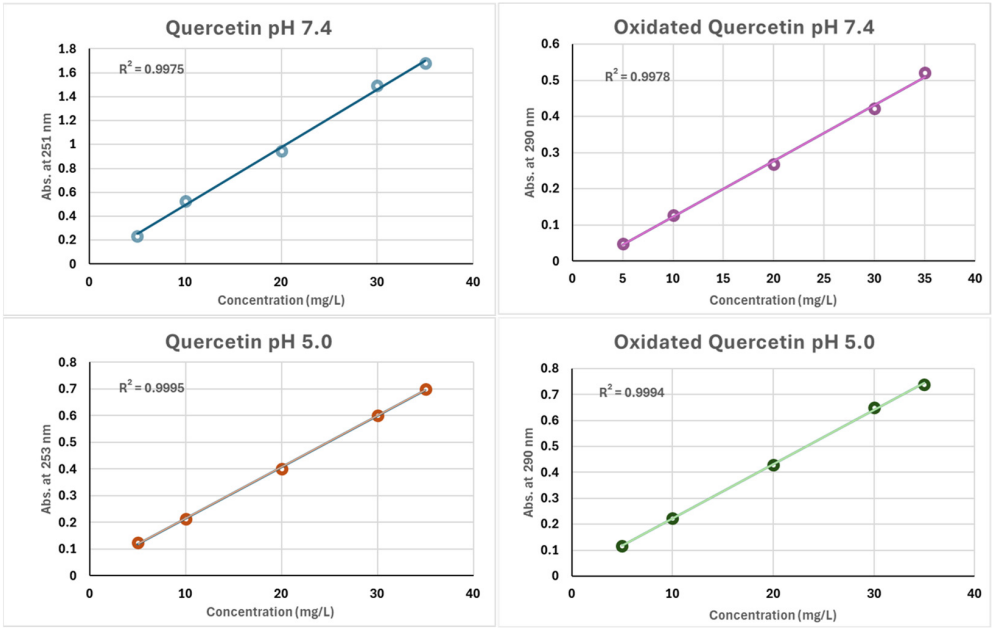

Figure 3. Calibration curve UV absorbance of quercetin and oxidated quercetin at pH 7.4 and 5.0.

2.2.4. Antimicrobial Study

An antimicrobial susceptibility test was employed according to the slight modification of the agar diffusion method reported by Kirby–Bauer [35]. This modification consists of using a round tablet of the synthesized sample (with a diameter of 1.3 cm) instead of using filters impregnated with antimicrobial solutions. This was carried out to explore the toxicity of the synthesized materials against various bacterial strains, known to cause nosocomial infections [36], grown both in the absence and the presence of the synthesized materials. *Escherichia coli* (ATCC 25922) and *Pseudomonas aeruginosa* (ATCC 27853) were utilized for the experiment as Gram-negative bacteria. The former was cultured on TBX Medium (Tryptone Bile X-Gluc) from Liofilchem, Italy, while the latter was cultured on Pseudomonas CN Agar. Concerning Gram-positive bacteria, *Staphylococcus aureus* (ATCC 25923) was cultured on Baird–Parker agar from Liofilchem, Italy, while *Enterococcus faecalis* (ATCC 29212) was cultivated on a Slanetz–Bartley agar base. The details regarding the preparation of media and samples are reported in [37]. Four measurements of the inhibition halo diameters were taken to calculate the mean standard deviation. Each sample was assayed three times per bacterial strain to validate the obtained data.

3. Results and Discussion

3.1. Structural Characterization of Si, Si-HNO_3, SiQ5, and SiQ5-HNO_3 Hybrid Materials

The influence study of the acid catalyst on the synthesis of Si and SiQ5 materials was carried out by means of a structural analysis through FTIR. In our previous paper, the addition of nitric acid during the sol-gel synthesis of the SiO_2 matrix to accelerate hydrolysis and polycondensation reactions contributed to the alteration of the quercetin structure. Indeed, it underwent an oxidation process with the alteration of the C-ring (Figure 1), resulting in the formation of a dihydroxybenzofuranone fraction because of the acidic environment experienced during synthesis [30].

The FTIR spectra of Si-HNO_3, SiQ5-HNO_3, and oxidated quercetin (Q Ox) are reported in Figure 4. In the spectrum of SiO_2-HNO_3, the bands at 796 and 460 cm^{-1} correspond to the bending vibrations of the Si–O–Si structure, along with the peak at 1078 cm^{-1} with a shoulder at 1210 cm^{-1} attributed to the symmetric and asymmetric stretching of the Si-O-Si bond. Moreover, the use of HNO_3 to accelerate the synthesis process was evident in the sharp peak at 1384 cm^{-1}, attributable to the NO_3^- group. The encapsulation of quercetin within the inorganic silicon matrix is highlighted in the SiQ5-HNO_3 spectrum by the presence of a peak at 1165 cm^{-1}, attributed to the stretching of the ketone group C–CO–C and the appearance of the peak at 1757 cm^{-1}, due to the carbonyl group's vibration of the flavonoid in a hydroxybenzofuranone structure [38,39], validated by NMR analysis conducted in our previous work [25]. The increase in the broadness of -OH stretching vibration at 3457 cm^{-1} is indicative of the formation of H-bonds between the hydroxyl group of the silanol group from the silica matrix and the -OH groups of entrapped quercetin. This was also demonstrated using a dynamic molecular approach [26], in which the interaction between the silica matrix and two amounts of quercetin, 5 and 15%, respectively, was simulated and discussed.

In Figure 5, the FTIR spectra of Si and SiQ5 synthesized via the sol-gel technique in the absence of nitric acid were reported using pure quercetin (Q in graph) for comparison. In the Si spectrum, unlike that synthesized in the acidic environment, sharp peaks indicate the residual presence of tetraethyl orthosilicate not completely hydrolyzed during the sol-gel process. Specifically, the peak at 1483 cm^{-1} is attributed to the OCH group. The peaks at 1447 and 1395 cm^{-1} could be attributed to the CH_3 group and the OCH/CCH groups, respectively, of residual TEOS or ethanol in the material [40]. The peak at 1087 cm^{-1} related to the Si-O-Si stretching exhibits a shift to higher wavenumbers, indicating a less advanced polycondensation process compared to that of Si-HNO_3 (1078 cm^{-1}). Furthermore, the peak at 1168 cm^{-1}, representing the CH_2 rocking of TEOS, is still slightly visible, also indicating an incomplete hydrolysis of TEOS, confirmed by the absence of the shoulder at 1210 cm^{-1} (which is present in Si-HNO_3, as shown in Figure 4), which increases with

the advancement of the polycondensation process [41]. The spectrum of SiQ5, despite the absence of nitric acid, does not show traces of unhydrolyzed TEOS. Additionally, it appears to have completed the process of polycondensation of SiO_2, as evidenced by the presence of the shoulder at approximately 1200 cm^{-1}. It is also observable that in this case, the encapsulation of quercetin does not lead to significant structural modifications of the quercetin. In fact, in the spectrum of SiQ5, the band at 1165 cm^{-1} is visible, overlapping with that of pure quercetin. Furthermore, there is a noticeable new broad band at 1740 cm^{-1}, which can be attributed to the stretching vibration of the carbonyl group within a six-membered-lactone structure [42]. The most plausible hypothesis would be the breakage of the double bond at positions 2–3 of the C-ring (see Q structure in Figure 1), resulting in the formation of a dihydroflavonol. Bondžić et al. also proposed a mechanism for the reaction between $[AuCl_4]^-$ and quercetin, highlighting that these reactions in the presence of water and alcohol lead to the formation of oxidation products where the double bond 2–3 in ring C is reduced [43].

To confirm the structural changes in quercetin encapsulated in the Si matrix in the presence of the acid catalyst and in the Si matrix synthesized without the catalyst, UV-vis spectra of quercetin extracted from the SiQ5-HNO_3 (Figure 6A) and SiQ5 (Figure 6B) systems were recorded.

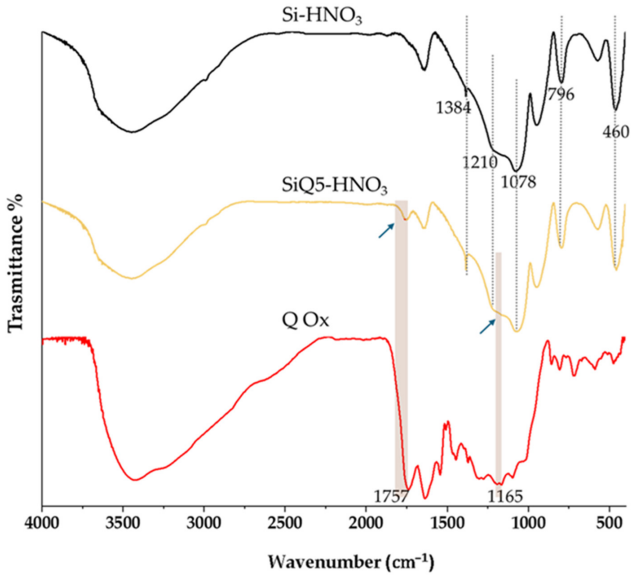

Figure 4. FTIR spectra of Si-HNO_3 and SiQ5-HNO_3, along with oxidated quercetin extracted from SiQ5-HNO_3. Blue arrows indicate peak position explained in main text.

Several studies have demonstrated that quercetin can undergo oxidation in the presence of an aqueous environment and acidic pH [44]. This oxidation process alters the flavonol skeleton, consequently affecting its antioxidant activity. It was therefore important to obtain further information about the structure of quercetin released from SiO_2 systems obtained through the sol-gel technique to assess if it maintains its biological activities. Pure quercetin, solubilized in a 2% ethanol physiological solution (SBF), shows two main characteristic bands: band I, located at 380 nm as the lambda maximum, generally attributed to the B–C rings system, which is a benzopyrone group, and band II at 250–260 nm, attributed to the cinnamoyl system [45]. Band I is due to a pure HOMO–LUMO transition, whereas band II results from a combination of several excitations [46]. During the oxidation of quercetin, as documented in various scientific studies, significant changes in the UV–visible spectrum occur. Initially, the characteristic absorption bands of quercetin at 250 nm and approximately 380 nm disappear, while a new band at 332 nm emerges, indicating the presence of the oxidation product after the removal of two electrons from the B-ring, forming a quinone structure. Additionally, there is an increase in absorption at 201 nm during

oxidation. In an advanced stage of oxidation, a band at about 290 nm appears, with a shoulder at 320 nm. This product is consistent with that obtained through the sol-gel synthesis of SiQ5-HNO_3 [47]. This finding is consistent with what was observed in this study. The entrapped quercetin undergoes an oxidation process that causes the opening and recyclization of the C-ring, causing a displacement of the quercetin absorption maximum (380 nm), resulting in a new peak with maximum absorbance at 295 nm with a shoulder at 320 nm (Figure 6A). This oxidation product presents a spectrum similar to that of the oxidation product 3(2H)-benzofuranone [48]. This product is obtained through the formation of a quinone derivative and subsequent chemical reactions such as hydroxylation [49]. A different behavior is observed for SiQ5, where, despite the absence of an added acidic catalyst, the presence of tetraethyl orthosilicate as SiO_2 precursors, conferring the synthesis solution a slightly acidic pH of about 5.0 along with a hydroalcoholic environment, caused a change in the initial structure of quercetin, as observed in Figure 6B, confirming what has already been observed in the FTIR SiQ5 spectrum. Specifically, a simultaneous decrease in band I (380 nm) and an increase in the 335 nm band are observed due to the breaking of the cinnamyl system (B- and C-rings) [50]. This absorption band is associated with the formation of quercetin o-quinoids during the oxidation reaction of quercetin, even though a specific structure for these compounds has not been definitively assigned [51].

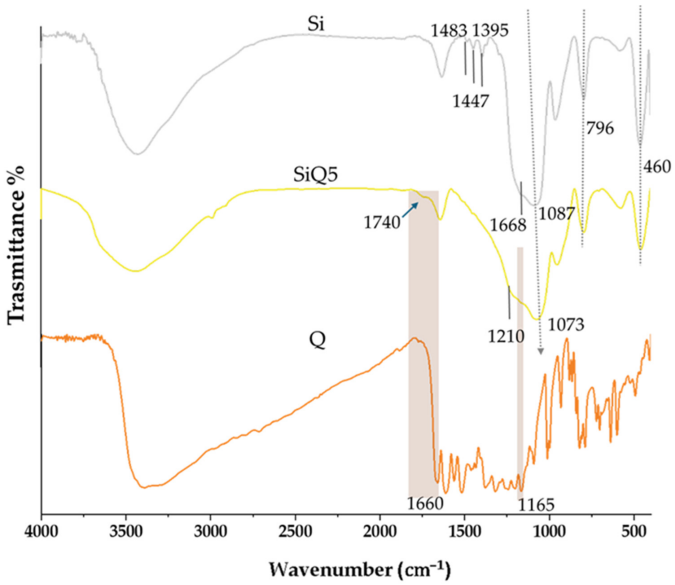

Figure 5. FTIR spectra of Si, SiQ5 and quercetin (Q). Arrows indicate peak position explained in the main text.

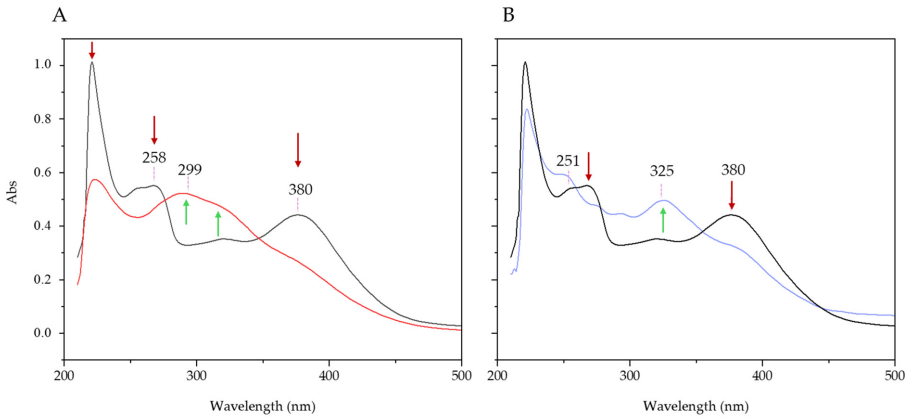

Figure 6. UV-vis spectra of quercetin extracted from SiQ5-HNO_3 ((**A**), in red line) and SiQ5 ((**B**), in blue line) with pure quercetin as a reference (black line). Arrows indicate peak positions.

The data from FTIR and UV–visible spectroscopy suggest that quercetin entrapped in both systems undergoes structural changes primarily due to the hydroalcoholic environment in which the synthesis takes place. The aqueous environment oxidizes the flavonol, causing modifications that involve the opening and recycling of the gamma-pyrene structure (ring C), which, in accordance with various scientific studies, leads to the loss of the double bond of quercetin at positions 2–3, interrupting the electronic resonance of the conjugated system between ring C and ring B. This results in a shift in the peak at 1660 cm^{-1} of the ketonic carbonyl (ring C) to higher wavenumbers—1757 cm^{-1} in the SiQ5-HNO_3 system and 1740 cm^{-1} in the SiQ5 system—as observed in the FTIR spectrum (Figure 7). These shifts can be attributed to the stretching vibration of the carbonyl in a five-membered lactonic ring (more strained structure) and in a six-membered lactonic ring (less strained structure, Figure 7). The UV spectra obtained from the extraction of quercetin released from the two synthesized systems confirm the structural changes compared to pure quercetin. The decrease in the 380 nm band observed in both systems is consistent with the loss of the conjugated system between ring C and ring B.

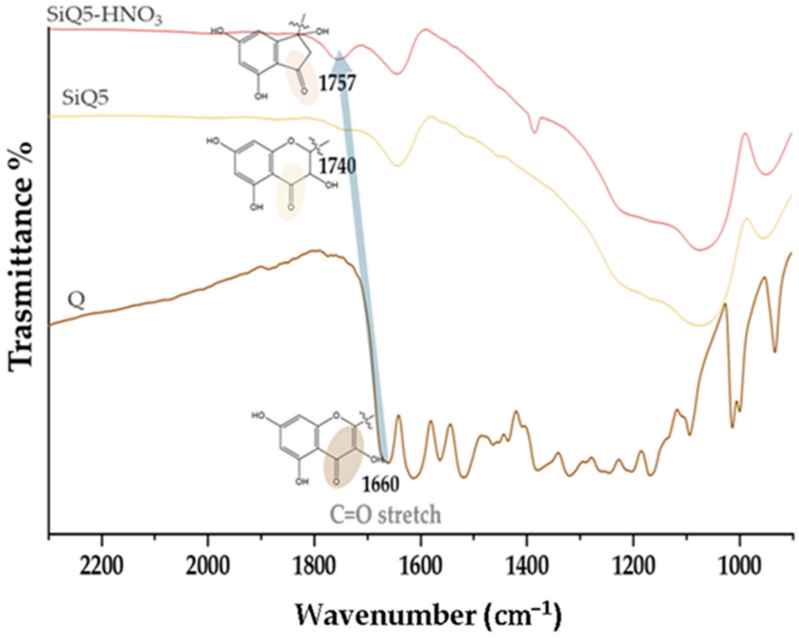

Figure 7. FTIR spectra of SiQ5, SiQ5-HNO_3, and standard quercetin in the carbonyl stretching band range and hypotheses of structural modifications of the C ring of quercetin. Blue arrow indicates peak shift.

3.2. Bioactivity Study

The bioactivity test was carried out to obtain information on the ability of the synthesized materials to allow hydroxyapatite formation on their surfaces after being soaked in SBF. This is an important feature to know, as it is strictly correlated with the first step of osteointegration [52,53]. In our case, hydroxyapatite formation was followed by FTIR signals by focusing on the 1100–400 cm^{-1} region, and SEM images, both acquired after 21 days of soaking (as shown in Figure 8). It has already been demonstrated that monitoring the formation of hydroxyapatite in the first weeks of soaking allows for assessing short-term bone regeneration progress. In particular, SiO_2-based materials can form hydroxyapatite as early as the day of implantation and continue to do so for up to 4 weeks, with a consistent increase over time [54], and after 21 days of soaking there is strong hydroxyapatite formation within a regular round shape. In our case, the spectra underlined for both the sample the presence of stretching and bending vibrations of phosphate groups (at 635, 560, and 470 cm^{-1}) [55,56], which were absent in the spectra of the as-synthesized samples (see Figures 4 and 5). Moreover, the SEM images revealed the presence of a typical

globular shape of hydroxyapatite structure [57], whose Ca/P ratios (see Table 1) from EDS analysis were 1.67 for the SiQ5-HNO_3 system and 1.73 for the SiQ5 system, respectively. The obtained values are close to those reported in the literature [58].

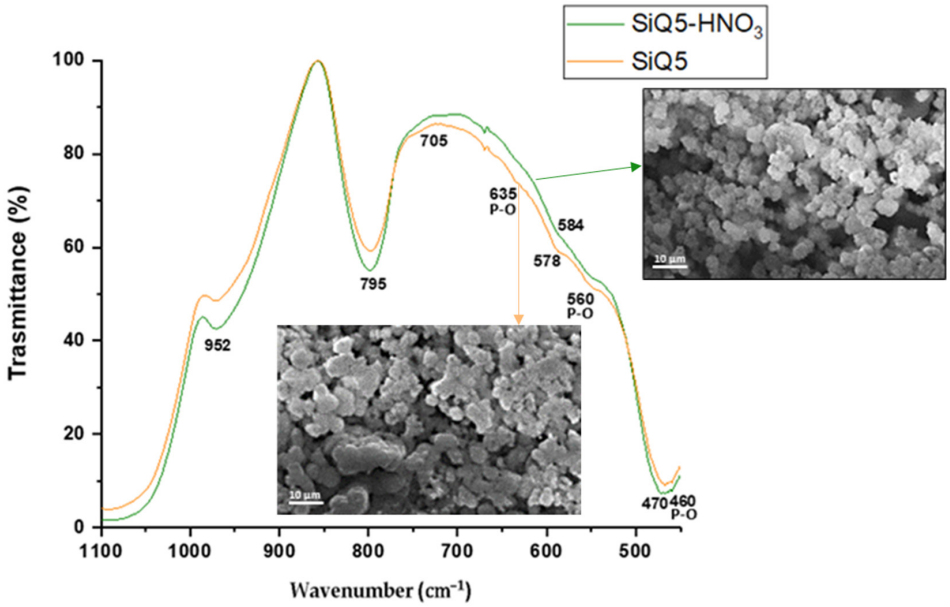

Figure 8. FTIR spectra of SiQ5 (orange line) and SiQ5-HNO_3 (green line) recorded in the range of 1100–400 cm^{-1} after 21 days of soaking in SBF and their respective SEM images.

Table 1. EDS data on Ca, O, and P weight percentages and calculated Ca/P ratios in SiQ5 and SiQ5-HNO_3 after 21 days of soaking in SBF.

Samples	EDS Measured Ca/P Ratio
SiQ5	1.73
SiQ5-HNO_3	1.67

3.3. Encapsulation Efficiency and In Vitro Release Study

The initial concentration of quercetin incorporated into the SiO_2 system was 5% with respect to the total amount of SiO_2 for both SiQ5 and SiQ-HNO_3. The encapsulation efficiency for both hybrid materials was evaluated to understand the real amount incorporated into the SiQ5 and SiQ5-HNO_3 systems and available for release. The results of encapsulation efficiency (EE%) are shown in Figure 9. The overall EE (%) was estimated to be 71.7 ± 2.15 for SiQ5, whereas for SiQ5-HNO_3, this value was 82.7 ± 3.9. These results suggest a high grade of drug incorporation for both systems, with a higher capacity for the silica system synthesized in the presence of the acid catalyst.

Successively, the drug release study was conducted for the SiQ5 and SiQ5-HNO_3 hybrid materials to investigate their capacity to act as drug delivery systems. For this purpose, the hybrid systems were incubated in simulated body fluid (SBF) at 37 °C, mimicking both a healthy physiological condition at pH 7.4 and a cancer-like condition at pH 5.0. The released quercetin was followed for 24 h, and the results were expressed as a percentage of the cumulative drug released relative to the maximum amount of quercetin incorporated into the matrix, as reported in Figure 10.

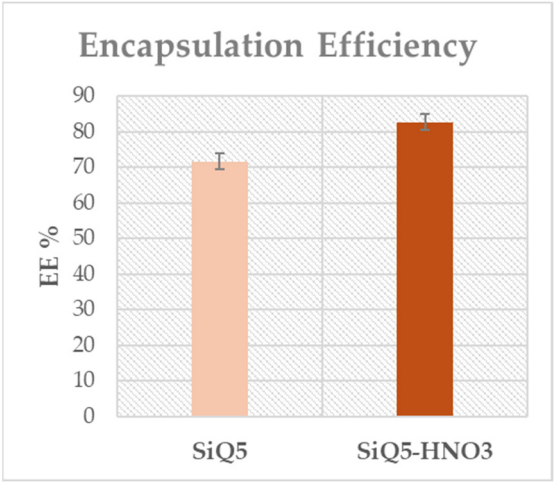

Figure 9. Encapsulation efficiency of quercetin inside SiQ5 and SiQ5-HNO_3 systems.

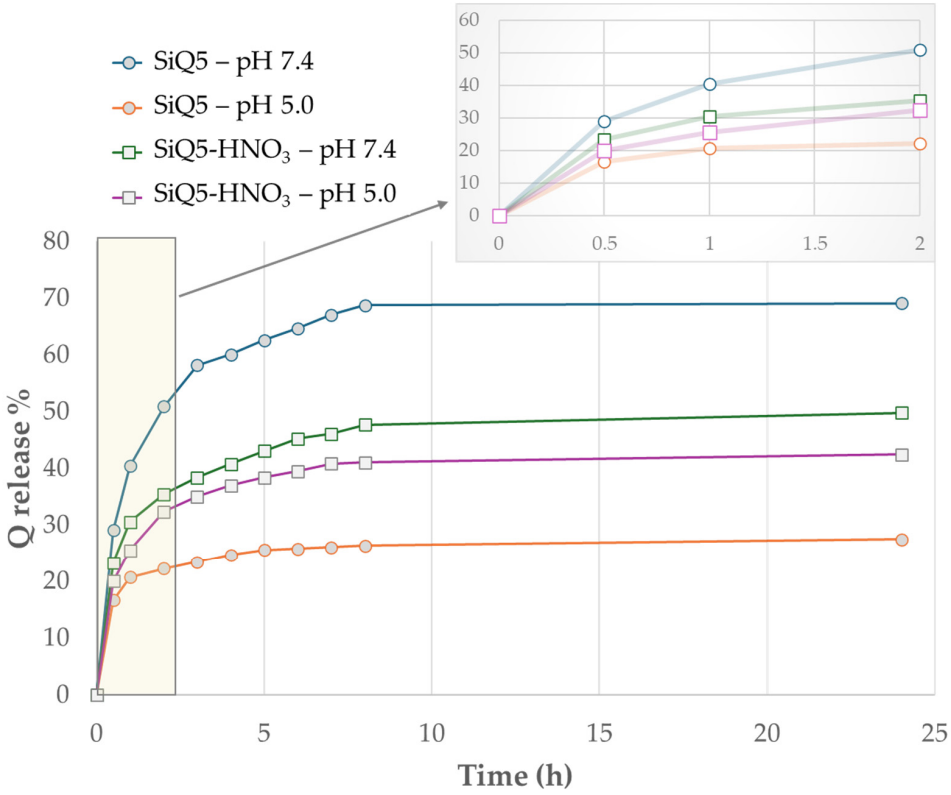

Figure 10. In vitro release study of SiQ5 and SiQ5-HNO_3 in SBF at pH 7.4 and 5.0.

For all materials, the release kinetics occur in two phases: an initial phase with a rapid release within the first two hours, regardless of the pH used for the test, corresponding to the desorption of drugs weakly interacting at the surface (burst release), and a second and slower phase corresponding to the diffusion of the flavonoid entrapped within the inner part of the clusters from the matrix to the physiological solution, as reported for other flavonoid drug delivery systems [44,59]. Curves in Figure 10 reveal that both the synthesized hybrid system and the pH employed for controlled release exert significant influence on the total percentage of released encapsulated quercetin. Specifically, at pH 7.4, the SiQ5 and SiQ5-HNO_3 systems demonstrate release rates of up to 69.05 and 49.78%, respectively. Conversely, under acidic conditions at pH 5.0, the cumulative percentage of quercetin released diminishes, reaching 27.46% for SiQ5. The SiQ5-HNO_3 system does not

show a significative difference between pH 7.4 and 5.0 release, indicating that the acidic environment does not substantially affect the release profile in this system. For pH 7.4, both systems reach a plateau after about 8 h of release, whereas for pH 5.0, it is reached after only 2 h. The release efficiency of quercetin can be controlled by pH, with a decrease in release as the pH value decreases, as reported in other studies [38,39]. At pH 5.0, the predominantly protonated functional groups of quercetin might closely interact with the silanol inorganic matrix, potentially slowing down drug release by limiting quercetin's availability to diffuse from the matrix. Conversely, at pH 7.4, the deprotonated functional groups of quercetin make the molecule less prone to interact with the inorganic matrix, thereby facilitating quercetin diffusion and increasing the drug release rate [60,61]. A higher drug release from matrices synthesized in the absence of an acid catalyst may be attributed to the differing porosity of the structure obtained during the synthesis process. The absence of an acid catalyst during the sol-gel synthesis of SiO_2 leads to a slower and less controlled formation of the matrix structure, resulting in a greater variety of pore sizes and distribution. This increased porosity facilitates drug release as it provides more space for the diffusion of drug molecules through the matrix. Conversely, the use of HNO_3 during synthesis results in the formation of a weakly branched -O-Si-O--based structure, characterized by a more closed and compact microstructure that partially impedes drug release [62]. Neither of the two systems is capable of fully releasing the encapsulated drug, indicating that a portion of the molecule is stacked in an inner part of the matrix in the form of aggregates, as previously reported in one of our earlier works [25]. After 24 h of the release test, pH values of the medium were calculated, and the results are reported in Table 2. The findings indicate that no pH variation occurred during the release process, confirming that the differential drug release capacity in the medium depended on structural differences in the inorganic matrix and the molecule subjected to oxidative processes rather than pH variations.

Table 2. pH value of samples after 24 h of kinetic release in SBF.

Sample	pH Value after 24 h Release
SiQ5 in SBF pH 7.4	7.47 ± 0.06
SiQ5 in SBF pH 5.0	5.20 ± 0.12
SiQ5-HNO_3 in SBF pH 7.4	7.43 ± 0.11
SiQ5-HNO_3 in SBF pH 5.0	4.80 ± 0.13

3.4. Antibacterial Activity

The SiO_2, SiO_2-HNO_3, SiQ5, and SiQ5-HNO_3 systems were tested against four bacterial strains (Figure 11). All systems exhibited an amount-dependent antimicrobial effect, but it was evident that the SiQ5-HNO_3 inhibition halos, compared with the other systems, were larger against all assayed bacteria (see orange curves in Figure 11). This enhanced antimicrobial activity is due to a combination of the presence of NO_3^- ions (whose residue's presence was confirmed by the characteristic nitrate stretching band in the relative FTIR spectrum) and the hydroxybenzofuranone structure derived from quercetin oxidation. Indeed, the former could be released in the form of nitrogen oxides during incubation with different bacterial strains, influencing the environment and affecting bacterial growth and vitality [63]. Indeed, studies have demonstrated that derivatives of nitric oxide (NO) can hinder bacterial growth and exert inhibitory effects on a wide range of bacteria, including Gram-negative, Gram-positive, and acid-resistant ones. This is due to NO's ability to easily diffuse through biological membranes. Once inside the bacterial cell, NO can interfere with vital processes such as DNA and protein synthesis [64,65]. Meanwhile, the latter acts as an antibacterial agent due to its benzofuran moiety, as the benzofuran structure with hydroxyl groups as substituents can interact with bacterial cellular structures, disrupting their vital processes and leading to cell death [66]. Moreover, the evidence of nitrates' antimicrobial effect can also be observed in the case of the SiO_2-HNO_3 system. Indeed, it

showed larger higher inhibition halo diameters (see blue curves in Figure 11), especially with respect to *P. aeruginosa* and *S. aureus*. The antimicrobial effect of this system was also better than that of the SiQ5 system (see yellow curves in Figure 11), which, in turn, showed an increase in the inhibition halo diameters compared the SiO_2 (Si) control. In this case, the higher antimicrobial activity can be related to the incorporated drug. Despite the loss of the C3-C2 double bond in the C ring (see Figure 7), which is well known for its involvement in antibacterial activity, the presence of polyhydroxybenzoic groups in the A and B rings remains essential for the antibacterial activity [67].

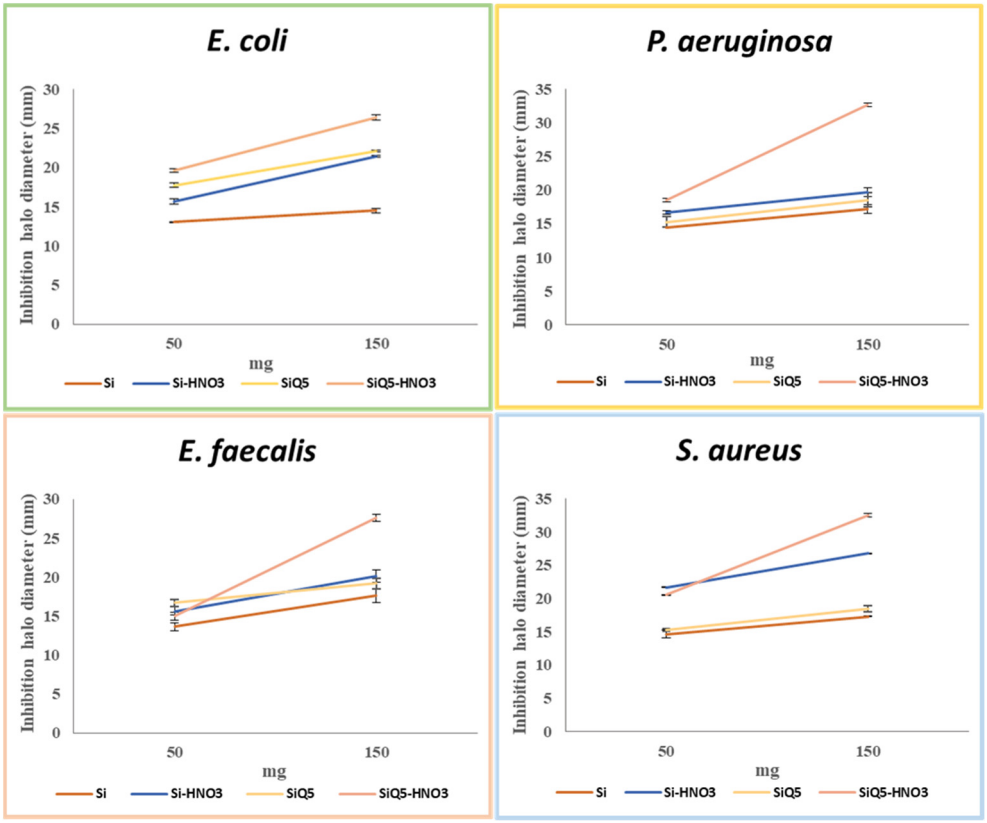

Figure 11. Measured inhibition halos after Si, Si-HNO_3, SiQ5, and SiQ5-HNO_3 incubation with the microbial strains.

4. Conclusions

The aim of this work was to synthesize a biomaterial in an eco-friendly manner, avoiding the use of acids and minimizing the generation of hazardous waste, while still retaining the desired characteristics of the material obtained with the acid catalyst. Our research findings demonstrate that it is possible to successfully synthesize an organic–inorganic hybrid system without the use of nitric acid as a catalyst, as confirmed by FTIR spectra. However, structural alterations affected the entrapped drug in both cases. In the presence of nitric acid, the quercetin oxidation forms 3(2H)-benzofuranone, while in its absence, oxidation in the hydroalcoholic synthesis environment resulted in the formation of a six-membered lactone ring. Both synthesized hybrid materials effectively promoted hydroxyapatite formation (as confirmed by FTIR analysis and SEM/EDS analysis), essential for osteointegration, with no significant differences observed between them. In vitro release studies demonstrated pH-dependent quercetin release, with a higher release capacity observed for the SiQ5 system compared to the SiQ5-HNO_3 system. This difference in release capacity was influenced by a different SiO_2 surface. However, the SiQ5-HNO_3 exhibited more effective antibacterial activity compared to SiQ5, likely due to the release of residual nitrate ions as well as the oxidated quercetin structure. These results highlight the

possibility of achieving a biomaterial with the desired properties without the use of acids. Further studies are necessary to improve the drug stability with any structural alteration (for example, Brunauer–Emmett–Teller (BET) theory could be useful to determine the specific surface area of the synthesized solid materials based on gas adsorption measurements, or magnetic nuclear resonance (NMR) could be used to strengthen molecular changes in quercetin's structure), as well as to understand the possible cytotoxicity and loss in antioxidant properties of modified quercetin. This ongoing research will contribute to the development of innovative biomaterials with improved performance and reduced environmental impact, ultimately benefiting various biomedical fields.

Author Contributions: Conceptualization, M.C. and A.D.; methodology, M.F. and A.D.; software, M.F. and V.V.; validation, M.F., A.D., V.V. and L.V.; formal analysis, M.F., A.D., V.V. and L.V.; investigation, M.F., V.V. and A.D.; resources, L.V.; data curation, M.F. and A.D.; writing—original draft preparation, A.D., M.F. and V.V.; writing—review and editing, all authors; visualization, L.V.; supervision, M.C.; project administration, M.C.; funding acquisition, M.C. All authors have read and agreed to the published version of the manuscript.

Funding: This research received no external funding.

Institutional Review Board Statement: Not applicable.

Informed Consent Statement: Not applicable.

Data Availability Statement: The original contributions presented in this study are included in this article; further inquiries can be directed to the corresponding author.

Acknowledgments: The authors thank the PRIN 2022 PNRR project #P2022S4TK2 GLASS-based TREAtments for Sustainable Upcycling of inorganic RESidues for the support in the antimicrobial tests. The authors also thank Ecoricerche Srl (Capua, Italy) for the SEM/EDS analysis.

Conflicts of Interest: The authors declare no conflicts of interest.

References

1. Xu, R.; Yin, J.; Li, L.; Hong, R.; Chen, Y.; Zhao, Q.; Zhou, Y.; Huang, T.; Lin, J. 3D-Printed Scaffolds of Porous Amorphous Calcium Phosphate Nanospheres Loaded with Quercetin for Promoting Bone Repair via Synergistic Osteogenesis and Immunoregulation. *ACS Appl. Nano Mater.* **2024**, *7*, 10573–10590. [CrossRef]
2. Tang, G.; Liu, Z.; Liu, Y.; Yu, J.; Wang, X.; Tan, Z.; Ye, X. Recent Trends in the Development of Bone Regenerative Biomaterials. *Front. Cell Dev. Biol.* **2021**, *9*, 665813. [CrossRef] [PubMed]
3. Dec, P.; Modrzejewski, A.; Pawlik, A. Existing and Novel Biomaterials for Bone Tissue Engineering. *Int. J. Mol. Sci.* **2023**, *24*, 529. [CrossRef] [PubMed]
4. Bharadwaz, A.; Jayasuriya, A.C. Recent trends in the application of widely used natural and synthetic polymer nanocomposites in bone tissue regeneration. *Mater. Sci. Eng. C Mater. Biol. Appl.* **2020**, *110*, 110698. [CrossRef] [PubMed]
5. Asri, R.I.M.; Harun, W.S.W.; Samykano, M.; Lah, N.A.C.; Ghani, S.A.C.; Tarlochan, F.; Raza, M.R. Corrosion and surface modification on biocompatible metals: A review. *Mater. Sci. Eng. C Mater. Biol. Appl.* **2017**, *1*, 1261–1274. [CrossRef] [PubMed]
6. Tanaka, T.; Komaki, H.; Chazono, M.; Kitasato, S.; Kakuta, A.; Akiyama, S.; Marumo, K. Basic research and clinical application of beta-tricalcium phosphate (β-TCP). *Morphologie* **2017**, *101*, 164–172. [CrossRef] [PubMed]
7. Al-Harbi, N.; Mohammed, H.; Al-Hadeethi, Y.; Bakry, A.S.; Umar, A.; Hussein, M.A.; Abbassy, M.A.; Vaidya, K.G.; Al Berakdar, G.; Mkawi, E.M.; et al. Silica-Based Bioactive Glasses and Their Applications in Hard Tissue Regeneration: A Review. *Pharmaceuticals* **2021**, *14*, 75. [CrossRef] [PubMed]
8. Deshmukh, K.; Kovářík, T.; Křenek, T.; Docheva, D.; Stich, T.; Pola, J. Recent advances and future perspectives of sol–gel derived porous bioactive glasses: A review. *RSC Adv.* **2020**, *10*, 33782–33835. [CrossRef] [PubMed]
9. Alvarez Echazú, M.I.; Renou, S.J.; Alvarez, G.S.; Desimone, M.F.; Olmedo, D.G. Synthesis and Evaluation of a Chitosan–Silica-Based Bone Substitute for Tissue Engineering. *Int. J. Molec. Sci.* **2022**, *23*, 13379. [CrossRef]
10. Song, Y.; Sun, Q.; Luo, J.; Kong, Y.; Pan, B.; Zhao, J.; Wang, Y.; Yu, C. Cationic and Anionic Antimicrobial Agents Co-Templated Mesostructured Silica Nanocomposites with a Spiky Nanotopology and Enhanced Biofilm Inhibition Performance. *Nano-Micro Lett.* **2022**, *14*, 83. [CrossRef]
11. Chen, L.; Zhang, S.; Duan, Y.; Song, X.; Chang, M.; Feng, W.; Chen, Y. Silicon-Containing Nanomedicine and Biomaterials: Materials Chemistry, Multi-Dimensional Design, and Biomedical Application. *Chem. Soc. Rev.* **2024**, *53*, 1167–1315. [CrossRef] [PubMed]
12. Brinker, C.J.; Scherer, G.W. *Sol-Gel Science: The Physics and Chemistry of Sol-Gel Processing*; Academic Press: Boston, MA, USA, 1990; ISBN 978-0-12-134970-7.

13. Innocenzi, P. Overview of the Sol–Gel Process. In *Springer Handbook of Aerogels*; Aegerter, M.A., Leventis, N., Koebel, M., Steiner Iii, S.A., Eds.; Springer Handbooks; Springer International Publishing: Cham, Switzerland, 2023; pp. 53–69. ISBN 978-3-030-27321-7.
14. Ciriminna, R.; Fidalgo, A.; Pandarus, V.; Béland, F.; Ilharco, L.M.; Pagliaro, M. The Sol–Gel Route to Advanced Silica-Based Materials and Recent Applications. *Chem. Rev.* **2013**, *113*, 6592–6620. [CrossRef] [PubMed]
15. Catauro, M.; D'Errico, Y.; D'Angelo, A.; Clarke, R.J.; Blanco, I. Antibacterial Activity and Iron Release of Organic-Inorganic Hybrid Biomaterials Synthesized via the Sol-Gel Route. *Appl. Sci.* **2021**, *11*, 9311. [CrossRef]
16. Vertuccio, L.; Guadagno, L.; D'Angelo, A.; Viola, V.; Raimondo, M.; Catauro, M. Sol-Gel Synthesis of Caffeic Acid Entrapped in Silica/Polyethylene Glycol Based Organic-Inorganic Hybrids: Drug Delivery and Biological Properties. *Appl. Sci.* **2023**, *13*, 2164. [CrossRef]
17. Chakraborty, P.K.; Adhikari, J.; Saha, P. Variation of the Properties of Sol–Gel Synthesized Bioactive Glass 45S5 in Organic and Inorganic Acid Catalysts. *Mater. Adv.* **2021**, *2*, 413–425. [CrossRef]
18. Bokov, D.; Turki Jalil, A.; Chupradit, S.; Suksatan, W.; Javed Ansari, M.; Shewael, I.H.; Valiev, G.H.; Kianfar, E. Nanomaterial by Sol-Gel Method: Synthesis and Application. *Adv. Mater. Sci. Eng.* **2021**, *2021*, 1–21. [CrossRef]
19. Pope, E.J.A.; Mackenzie, J.D. Sol-Gel Processing of Silica. *J. Non Cryst. Solids* **1986**, *87*, 185–198. [CrossRef]
20. Fuentes, J.; Atala, E.; Pastene, E.; Carrasco-Pozo, C.; Speisky, H. Quercetin Oxidation Paradoxically Enhances Its Antioxidant and Cytoprotective Properties. *J. Agric. Food Chem.* **2017**, *65*, 11002–11010. [CrossRef] [PubMed]
21. Pérez, H.; Miranda, R.; Saavedra-Leos, Z.; Zarraga, R.; Alonso, P.; Moctezuma, E.; Martínez, J. Green and Facile Sol–Gel Synthesis of the Mesoporous SiO_2 –TiO_2 Catalyst by Four Different Activation Modes. *RSC Adv.* **2020**, *10*, 39580–39588. [CrossRef]
22. Das, S.S.; Hussain, A.; Verma, P.R.P.; Imam, S.S.; Altamimi, M.A.; Alshehri, S.; Singh, S.K. Recent Advances in Liposomal Drug Delivery System of Quercetin for Cancer Targeting: A Mechanistic Approach. *CDD* **2020**, *17*, 845–860. [CrossRef]
23. Michala, A.-S.; Pritsa, A. Quercetin: A Molecule of Great Biochemical and Clinical Value and Its Beneficial Effect on Diabetes and Cancer. *Diseases* **2022**, *10*, 37. [CrossRef] [PubMed]
24. Li, Y.; Yao, J.; Han, C.; Yang, J.; Chaudhry, M.; Wang, S.; Liu, H.; Yin, Y. Quercetin, Inflammation and Immunity. *Nutrients* **2016**, *8*, 167. [CrossRef] [PubMed]
25. Petrelli, V.; Dell'Anna, M.M.; Mastrorilli, P.; Viola, V.; Catauro, M.; D'Angelo, A. Synthesis by Sol–Gel Route of Organic–Inorganic Hybrid Material: Chemical Characterization and In vitro Release Study. *Appl. Sci.* **2023**, *13*, 8410. [CrossRef]
26. Raffaini, G.; Pirozzi, P.; Catauro, M.; D'Angelo, A. Hybrid Organic–Inorganic Biomaterials as Drug Delivery Systems: A Molecular Dynamics Study of Quercetin Adsorption on Amorphous Silica Surfaces. *Coatings* **2024**, *14*, 234. [CrossRef]
27. Trzeciak, K.; Chotera-Ouda, A.; Bak-Sypien, I.I.; Potrzebowski, M.J. Mesoporous Silica Particles as Drug Delivery Systems—The State of the Art in Loading Methods and the Recent Progress in Analytical Techniques for Monitoring These Processes. *Pharmaceutics* **2021**, *13*, 950. [CrossRef] [PubMed]
28. Andreani, T.; De Souza, A.L.R.; Silva, A.M.; Souto, E.B. Sol–Gel Carrier System: A Novel Controlled Drug Delivery. In *Patenting Nanomedicines*; Souto, E.B., Ed.; Springer Berlin Heidelberg: Berlin/Heidelberg, Germany, 2012; pp. 151–166. ISBN 978-3-642-29264-4.
29. Owens, G.J.; Singh, R.K.; Foroutan, F.; Alqaysi, M.; Han, C.-M.; Mahapatra, C.; Kim, H.-W.; Knowles, J.C. Sol–Gel Based Materials for Biomedical Applications. *Prog. Mater. Sci.* **2016**, *77*, 1–79. [CrossRef]
30. Catauro, M.; D'Angelo, A.; Fiorentino, M.; Pacifico, S.; Latini, A.; Brutti, S.; Vecchio Ciprioti, S. Thermal, Spectroscopic Characterization and Evaluation of Antibacterial and Cytotoxicity Properties of Quercetin-PEG-Silica Hybrid Materials. *Ceram. Int.* **2023**, *49*, 14855–14863. [CrossRef]
31. Kokubo, T.; Takadama, H. How Useful Is SBF in Predicting in Vivo Bone Bioactivity? *Biomaterials* **2006**, *27*, 2907–2915. [CrossRef] [PubMed]
32. Li, W.; Chen, J.; Zhao, S.; Huang, T.; Ying, H.; Trujillo, C.; Molinaro, G.; Zhou, Z.; Jiang, T.; Liu, W.; et al. High drug-loaded microspheres enabled by controlled in-droplet precipitation promote functional recovery after spinal cord injury. *Nat. Commun.* **2022**, *13*, 1262. [CrossRef]
33. Piacentini, E. Encapsulation Efficiency. In *Encyclopedia of Membranes*; Drioli, E., Giorno, L., Eds.; Springer: Berlin/Heidelberg, Germany, 2016. [CrossRef]
34. Jackson, N.; Ortiz, A.C.; Jerez, A.; Morales, J.; Arriagada, F. Kinetics and Mechanism of Camptothecin Release from Transferrin-Gated Mesoporous Silica Nanoparticles through a pH-Responsive Surface Linker. *Pharmaceutics* **2023**, *15*, 1590. [CrossRef]
35. Hudziky, J. Kirby-Bauer Disk Diffusion Susceptibility Test Protocol. *Am. Soc. Microbiol.* **2009**, *15*, 55–63.
36. Caruso, A.A.; Viola, V.; Del Prete, S.; Leo, S.; Marasco, D.; Fulgione, A.; Naviglio, D.; Gallo, M. Identification and Characterization of Nasal Polyposis and Mycoplasma Superinfection by Scanning Electron Microscopy and Nasal Cytology with Optical Microscopy: A Case Report. *Diagnostics* **2019**, *9*, 174. [CrossRef] [PubMed]
37. Righi, C.; Barbieri, F.; Sgarbi, E.; Maistrello, L.; Bertacchini, A.; Andreola, F.N.; D'Angelo, A.; Catauro, M.; Barbieri, L. Suitability of Porous Inorganic Materials from Industrial Residues and Bioproducts for Use in Horticulture: A Multidisciplinary Approach. *Appl. Sci.* **2022**, *12*, 5437. [CrossRef]
38. Saputra, O.A.; Lestari, W.A.; Kurniansyah, V.; Lestari, W.W.; Sugiura, T.; Mukti, R.R.; Martien, R.; Wibowo, F.R. Organically Surface Engineered Mesoporous Silica Nanoparticles Control the Release of Quercetin by pH Stimuli. *Sci. Rep.* **2022**, *12*, 20661. [CrossRef] [PubMed]

39. AbouAitah, K.E.A.; Farghali, A.A.; Swiderska-Sroda, A.; Lojkowski, W.; Razin, A.M.; Khedr, M.K. Mesoporous Silica Materials in Drug Delivery System: pH/Glutathione- Responsive Release of Poorly Water-Soluble Pro-Drug Quercetin from Two and Three-Dimensional Pore-Structure Nanoparticles. *J. Nanomed. Nanotechnol.* **2016**, *7*, 1000360. [CrossRef]
40. Mondragón, M.A.; Castaño, V.M.; Garcia, M.J.; Téllez, S.C.A. Vibrational Analysis of Si(OC2H5)4 and Spectroscopic Studies on the Formation of Glasses via Silica Gels. *Vib. Spectrosc.* **1995**, *9*, 293–304. [CrossRef]
41. Rubio, F.; Rubio, J.; Oteo, J.L. A FT-IR Study of the Hydrolysis of Tetraethylorthosilicate (TEOS). *Spectrosc. Lett.* **1998**, *31*, 199–219. [CrossRef]
42. Silverstein, R.M.; Webster, F.X.; Kiemle, D.J.; Bryce, D.L. *Spectrometric Identification of Organic Compounds*, 8th ed.; Wiley: Hoboken, NJ, USA, 2015; ISBN 978-0-470-61637-6.
43. Bondžić, A.M.; Lazarević-Pašti, T.D.; Bondžić, B.P.; Čolović, M.B.; Jadranin, M.B.; Vasić, V.M. Investigation of Reaction between Quercetin and Au(Iii) in Acidic Media: Mechanism and Identification of Reaction Products. *New J. Chem.* **2013**, *37*, 901. [CrossRef]
44. Dall'Acqua, S.; Miolo, G.; Innocenti, G.; Caffieri, S. The Photodegradation of Quercetin: Relation to Oxidation. *Molecules* **2012**, *17*, 8898–8907. [CrossRef]
45. Zhai, G.; Zhu, W.; Duan, Y.; Qu, W.; Yan, Z. Synthesis, characterization and antitumor activity of the germanium-quercetin complex. *Main Group Met. Chem.* **2012**, *35*, 103–109. [CrossRef]
46. Skoko, S.; Ambrosetti, M.; Giovannini, T.; Cappelli, C. Simulating Absorption Spectra of Flavonoids in Aqueous Solution: A Polarizable QM/MM Study. *Molecules* **2020**, *25*, 5853. [CrossRef] [PubMed]
47. Sokolová, R.; Degano, I.; Ramešová, Š.; Bulíčková, J.; Hromadová, M.; Gál, M.; Fiedler, J.; Valášek, M. The oxidation mechanism of the antioxidant quercetin in nonaqueous media. *Electrochim. Acta* **2011**, *56*, 7421–7427. [CrossRef]
48. Jørgensen, L.V.; Cornett, C.; Justesen, U.; Skibsted, L.H.; Dragsted, L.O. Two-Electron Electrochemical Oxidation of Quercetin and Kaempferol Changes Only the Flavonoid C-Ring. *Free. Radic. Res.* **1998**, *29*, 339–350. [CrossRef] [PubMed]
49. Ramešová, Š.; Sokolová, R.; Degano, I.; Bulíčková, J.; Žabka, J.; Gál, M. On the Stability of the Bioactive Flavonoids Quercetin and Luteolin under Oxygen-Free Conditions. *Anal. Bioanal. Chem.* **2012**, *402*, 975–982. [CrossRef] [PubMed]
50. Zhou, A.; Sadik, O.A. Comparative Analysis of Quercetin Oxidation by Electrochemical, Enzymatic, Autoxidation, and Free Radical Generation Techniques: A Mechanistic Study. *J. Agric. Food Chem.* **2008**, *56*, 12081–12091. [CrossRef] [PubMed]
51. Metodiewa, D.; Jaiswal, A.K.; Cenas, N.; Dickancaité, E.; Segura-Aguilar, J. Quercetin May Act as a Cytotoxic Prooxidant after Its Metabolic Activation to Semiquinone and Quinoidal Product. *Free. Radic. Biol. Med.* **1999**, *26*, 107–116. [CrossRef] [PubMed]
52. Mujahid, M.; Sarfraz, S.; Amin, S. On the Formation of Hydroxyapatite Nano Crystals Prepared Using Cationic Surfactant. *Mat. Res.* **2015**, *18*, 468–472. [CrossRef]
53. Lee, S.-W.; Kim, S.-G.; Balázsi, C.; Chae, W.-S.; Lee, H.-O. Comparative Study of Hydroxyapatite from Eggshells and Synthetic Hydroxyapatite for Bone Regeneration. *Oral Surg. Oral Med. Oral Pathol. Oral Radiol.* **2012**, *113*, 348–355. [CrossRef] [PubMed]
54. Catauro, M.; Papale, F.; Roviello, G.; Ferone, C.; Bollino, F.; Trifuoggi, M.; Aurilio, C. Synthesis of SiO_2 and CaO rich calcium silicate systems via sol-gel process: Bioactivity, biocompatibility, and drug delivery tests. *J. Biomed. Mater. Res. Part A* **2014**, *102A*, 3087–3092. [CrossRef]
55. Sahadat Hossain, M.; Ahmed, S. FTIR Spectrum Analysis to Predict the Crystalline and Amorphous Phases of Hydroxyapatite: A Comparison of Vibrational Motion to Reflection. *RSC Adv.* **2023**, *13*, 14625–14630. [CrossRef]
56. Vechietti, F.A.; Marques, D.; Muniz, N.O.; Santos, L.A. Fibers Obtaining and Characterization Using Poly (Lactic-Co-Glycolic Acid) and Poly (Isoprene) Containing Hydroxyapatite and α TCP Calcium Phosphate by Electrospinning Method. *KEM* **2014**, *631*, 173–178. [CrossRef]
57. Liu, X.; He, D.; Zhou, Z.; Wang, Z.; Wang, G. The Influence of Process Parameters on the Structure, Phase Composition, and Texture of Micro-Plasma Sprayed Hydroxyapatite Coatings. *Coatings* **2018**, *8*, 106. [CrossRef]
58. Singh, R.; Tan, C.; Abd Shukor, M.; Sopyan, I.; Teng, W. The Influence of Ca/P Ratio on the Properties of Hydroxyapatite Bioceramics. In Proceedings of the International Conference on Smart Materials and Nanotechnology in Engineering A, Harbin, China, 1–4 July 2007; Proceedings SPIE: Bellingham, WA, USA, 2007; Volume 6423. [CrossRef]
59. Sadžak, A.; Eraković, M.; Šegota, S. Kinetics of Flavonoid Degradation and Controlled Release from Functionalized Magnetic Nanoparticles. *Mol. Pharm.* **2023**, *20*, 5148–5159. [CrossRef] [PubMed]
60. Belton, D.J.; Deschaume, O.; Perry, C.C. An Overview of the Fundamentals of the Chemistry of Silica with Relevance to Biosilicification and Technological Advances. *FEBS J.* **2012**, *279*, 1710–1720. [CrossRef] [PubMed]
61. Papan, P.; Kantapan, J.; Sangthong, P.; Meepowpan, P.; Dechsupa, N. Iron (III)-Quercetin Complex: Synthesis, Physicochemical Characterization, and MRI Cell Tracking toward Potential Applications in Regenerative Medicine. *Contrast Media Mol. Imaging* **2020**, *2020*, 1–22. [CrossRef] [PubMed]
62. Huck-Iriart, C.; Morales, N.J.; Herrera, M.L.; Candal, R.J. Micro to Mesoporous SiO2xerogels: The Effect of Acid Catalyst Type in Sol–Gel Process. *J. Sol Gel Sci. Technol.* **2022**, *102*, 197–207. [CrossRef]
63. Takeda, Y.; Hashimoto, T.; Nasu, H.; Kamiya, K. Crystallization Behavior of Alumina Gels Prepared by Sol-Gel Method Using Nitric Acid as a Catalyst. Complete .ALPHA.-Transformation at 800.DEG.C.: Complete α-Transformation at 800 °C. *J. Ceram. Soc. Jpn.* **2002**, *110*, 1025–1028. [CrossRef]
64. Chen, J.; Liu, L.; Wang, W.; Gao, H. Nitric Oxide, Nitric Oxide Formers and Their Physiological Impacts in Bacteria. *Int. J. Mol. Sci.* **2022**, *23*, 10778. [CrossRef] [PubMed]

65. Bath, P.M.; Coleman, C.M.; Gordon, A.L.; Lim, W.S.; Webb, A.J. Nitric Oxide for the Prevention and Treatment of Viral, Bacterial, Protozoal and Fungal Infections. *F1000Research* **2021**, *10*, 536. [CrossRef]
66. Hiremathad, A.; Patil, M.R.; Chethana, K.R.; Chand, K.; Santos, M.A.; Keri, R.S. Benzofuran: An emerging scaffold for antimicrobial agents. *RSC Adv.* **2015**, *5*, 96809–96828. [CrossRef]
67. Shamsudin, N.F.; Ahmed, Q.U.; Mahmood, S.; Ali Shah, S.A.; Khatib, A.; Mukhtar, S.; Alsharif, M.A.; Parveen, H.; Zakaria, Z.A. Antibacterial Effects of Flavonoids and Their Structure-Activity Relationship Study: A Comparative Interpretation. *Molecules* **2022**, *27*, 1149. [CrossRef] [PubMed]

Disclaimer/Publisher's Note: The statements, opinions and data contained in all publications are solely those of the individual author(s) and contributor(s) and not of MDPI and/or the editor(s). MDPI and/or the editor(s) disclaim responsibility for any injury to people or property resulting from any ideas, methods, instructions or products referred to in the content.